The Astronomical Journal, 156:278 (9pp), 2018 December https://doi.org/10.3847/1538-3881/aaeacb

The Araucaria Project: Multi-band Calibrations of the TRGB Absolute Magnitude

Marek Górski[1,2], Grzegorz Pietrzyński[1,3], Wolfgang Gieren[1,2], Dariusz Graczyk[1,2,3], Ksenia Suchomska[1,4], Paulina Karczmarek[4], Roger E. Cohen[1,5], Bartłomiej Zgirski[3], Piotr Wielgórski[3], Bogumił Pilecki[1,3], Mónica Taormina[3], Zbigniew Kołaczkowski[3], and Weronika Narloch[1,2,3]

[1] Universidad de Concepcíoon, Departamento de Astronomia, Casilla 160-C, Concepcíoon, Chile; mgorski@astro-udec.cl
[2] Millennium Astrophysical Institute, Santiago, Chile
[3] Nicolaus Copernicus Astronomical Center, Polish Academy of Sciences, Bartycka 18, 00-716, Warsaw, Poland
[4] Warsaw University Observatory, Al. Ujazdowskie 4, 00-478, Warsaw, Poland
[5] Space Telescope Science Institute, 3700 San Martin Drive, Baltimore, MD 21218, USA
Received 2018 August 5; revised 2018 October 1; accepted 2018 October 21; published 2018 November 28

Abstract

We present new empirical calibrations of the absolute magnitude of the tip of the red giant branch (TRGB) in the optical I and near-infrared J, H, and K bands in terms of the $(V-K)_0$, $(V-H)_0$, and $(J-K)_0$ colors of the red giant branch (RGB). Our calibrations are based on the measurements in 19 fields in the Large and Small Magellanic Clouds, which span a wide $(V-K)_0$ color range of the brightest part of the RGB. We use a simple edge detection technique based on the comparison of the star count difference in two adjacent bins with the estimated Poisson noise. Further, we include the reddening and geometrical corrections, as well as the distance to the Large Magellanic Cloud that is precise and accurate to within 2%. The calibration based on $(V-K)$ colors can be a robust tool to calculate the absolute magnitude of the TRGB with great precision.

Key words: distance scale – Magellanic Clouds – stars: distances – stars: late-type

1. Introduction

In recent years, a lot of attention was put on distance measurements and on improving the calibration of the distance scale (Beaton et al. 2016; Riess et al. 2016). In our long-term Araucaria Project, we have investigated and applied most of the precise distance measurement methods, like the mean brightness of the red clump stars (Pietrzyński & Gieren 2002; Pietrzyński et al. 2010), Cepheid period–luminosity (P–L) relation (Gieren et al. 2005; Wielgórski et al. 2017; Zgirski et al. 2017), RR Lyrae stars (Szewczyk et al. 2009; Karczmarek et al. 2017), late-type eclipsing binaries (Pietrzyński et al. 2009b; Graczyk et al. 2018), and blue supergiants (Berger et al. 2018; Urbaneja et al. 2008). In this paper, we continue our investigations on the tip of the red giant branch (TRGB) method (Pietrzyński et al. 2009a; Górski et al. 2011; Górski et al. 2016).

The TRGB is the sharp cut-off on the color–magnitude diagram occurring at the bright end of the red giant branch (RGB). It marks the final stage of the evolution of stars during the RGB phase, which is terminated by a helium flash. Because all low-mass stars have a similar I band brightness just before the helium flash, and this brightness very weakly depends on the stellar mass and age for old metal-poor stellar populations, the I band magnitude of the TRGB can be used as a standard candle (Madore & Freedman 1995; Barker et al. 2004).

The idea of using the TRGB to measure the distance was first used by Baade (1944a). With red-sensitive photographic plates, he observed the central region of the Andromeda galaxy and its two companion galaxies, M32 and NGC 205. He noticed that the brightest red giants in all three galaxies have the same magnitude and color. Moreover, he stated that the galaxies NGC 147 and NGC 185 should be at the same distance as the Andromeda system, since the brightest red stars in those galaxies also have a similar magnitude as the stars in the Andromeda system (Baade 1944b). Sandage (1971) found that the brightest red stars in the IC 1613 galaxy have the same absolute magnitude as in the M31 and M33 galaxies.

Over the subsequent decades, more sophisticated techniques to measure the brightness of the TRGB were developed, and with the arrival of CCD measurements, the TRGB brightness was used to determine the distances to almost all Local Group galaxies. With those measurements, many different investigations were conducted to check the reliability of the TRGB method. It became clear that the I band TRGB brightness depends on the RGB metallicity at the level of 0.1 mag. This dependence was calibrated by Da Costa & Armandroff (1990). In the same paper, the authors presented a relation to calculate the metallicity from the $(V-I)$ color of the RGB, which was the first indirect calibration of the TRGB absolute I band brightness from the color of the RGB.

In 1993, Lee et al. compared the distances obtained with the TRGB I band brightness with distances obtained with the Cepheid P–L relation and RR Lyrae stars for 10 Local Group galaxies. The obtained distances agree within 0.2 mag, proving that the TRGB method can be successfully applied to measure the distance. Until now, the TRGB method was applied to determine the distances to more than 300 galaxies up to 16 Mpc (Jacobs et al. 2009; Tully et al. 2016; Hatt et al. 2018).

Since metallicity measurements are scarce, most calibrations are based on the $(V-I)$ color of the RGB (Rizzi et al. 2007; Jacobs et al. 2009). Very recently Jang & Lee (2017) calibrated the optical I band absolute magnitude of the TRGB in terms of the F814W–F555W color, which is the Advanced Camera for Surveys/WFC *Hubble Space Telescope* equivalent of the $(V-I)$ color. The zero-point of this calibration is based on two distance anchors, NGC 4258 (M106) and the LMC. The advantage of this approach lies in the fact that the precise geometrical distances to both galaxies are known (Herrnstein et al. 1999; Pietrzyński et al. 2013).

One of the biggest contributions to the total uncertainty of the distances measured with the TRGB in the I band comes from the interstellar extinction. Usually only the Galactic foreground reddening is taken into account and the internal extinction is assumed to be negligible. This approach is justified as long, as the observations are performed in the halo of the galaxies, which is presumably dust free. In some cases, this assumption can lead to systematic errors. In recent years, our group measured the distance and reddening to a number of Local Group galaxies based on the near-infrared photometry of Cepheid variables. We found that the total reddening tends to by systematically higher compared to the Galactic foreground reddening. If the TRGB stars are affected from the internal reddening in a similar way as Cepheids, the reddening underestimation by 0.05 mag will lead to a distance moduli overestimation in the I band by 0.06 mag. (Gieren et al. 2005, 2006, 2008, 2009, 2013; Pietrzyński et al. 2006; Soszyński et al. 2006; Zgirski et al. 2017).

The effect of reddening can be reduced by utilizing near-infrared bands. In 2004, Valenti, Ferraro, & Origlia calibrated the TRGB infrared J, H, and K absolute brightnesses in terms of metallicity. In the last 10 years, this calibration was applied to measure the distance to only a few galaxies (Górski et al. 2011). The main disadvantage of this method is a strong sensitivity of the near-infrared bands to metallicity (a 0.1 dex metallicity difference changes the brightness of the TRGB in the K band by 0.058 mag), in tandem with scarce spectroscopic metallicity measurements (Cohen et al. 2017).

In our last paper (Górski et al. 2016), we empirically confirmed that the metallicity-dependent calibration of Valenti et al. (2004) leads to systematic errors at the level of 0.2 mag, if applied to the Large and Small Magellanic Clouds (LMC and SMC, respectively). This problem was already confirmed by many theoretical studies (Barker et al. 2004; Salaris & Girardi 2005; Serenelli et al. 2017) and is caused by population effects, namely the age and chemical composition of the red giants. In contrast to metallicity-dependent calibrations, the color–TRGB absolute magnitude relations are much less affected by this systematic error (Górski et al. 2016; Serenelli et al. 2017).

Recently, both theoretical and empirical calibrations of the infrared TRGB brightness in terms of the $(J - K)$ and $(J - H)$ colors were published. Serenelli et al. (2017) provided a solid theoretical calibration based on a careful stellar modeling. Hoyt et al. (2018) and Madore et al. (2018) derived the empirical near-infrared calibrations of the TRGB based on the LMC distance and slope of the TRGB observed in the IC 1613 dwarf galaxy.

Motivated by these results, we decided to independently calibrate the TRGB absolute magnitude, taking advantage of the wide color spread observed in different fields in the LMC and SMC, and the accurate geometrical distances to both galaxies measured recently with the eclipsing binaries method. While our focus is on the $(V - K)$ color that allows us to calculate the absolute brightness of the TRGB with great precision, we also investigate the $(V - H)$ and $(J - K)$ color calibrations.

During the last decade, the TRGB method and Cepheid P–L relation were used to calibrate the absolute magnitudes of supernovae Ia (SNe Ia) in nearby galaxies, and determine the value of the Hubble constant. In comparison with the Cepheid P–L relation, the TRGB was used to measure the distance to a much larger number of galaxies, including galaxies that lack young standard candles like classical Cepheids. Cepheid distance measurements are also affected by numerous systematic errors including reddening, a possible metallicity dependence, or a nonlinearity of the P–L relation (Kodric et al. 2015). Therefore, the TRGB method is an important tool that can complement and perhaps improve the determination of the Hubble parameter.

Our paper is organized as follows. The data sources, edge detection technique, and the TRGB and color measurements are described in the following section. In Section 3, we present the resulting calibrations. Results are discussed in Section 4. Finally we present a summary and conclusions.

2. Data Analysis

The optical V and I band photometry of the stars in the LMC and SMC were acquired from the photometric maps of the OGLE-III survey (Udalski et al. 2008a, 2008b). The OGLE-III photometric maps were obtained with the 1.3 m Warsaw telescope located at the Las Campanas Observatory. The telescope was equipped with a mosaic camera with a 0.26 arcsec pixel scale. The V and I band magnitudes were calibrated onto the standard system using Landolt standards. The source of the near-infrared J, H, and K band brightnesses is the IRSF Magellanic Clouds Point Source Catalog (Kato et al. 2007). The IRSF is a 1.4 m telescope, located at the South African Astronomical Observatory, equipped with the SIRIUS camera (0.45 arcsec pixel scale). The photometric system consists of three near-infrared filters similar to the 2MASS and UKIRT photometric systems. This allowed us to transform the magnitudes onto the 2MASS NIR photometric system following the procedure described by Kato et al. (2007). The optical V and I band catalog of OGLE-III was crossmatched with the IRSF near-infrared catalog based on the provided coordinates. The statistical photometric uncertainty of stars that were used in our analysis is 0.03 mag for the V band, and below 0.02 mag for the I, J, H, and K bands. To estimate the systematic error on the photometry, we decided to crossmatch the brightest stars with the 2MASS catalog (Skrutskie et al. 2006). The mean magnitude difference between our transformed IRSF brightnesses and the 2MASS catalog is below 0.01 mag for all bands.

The photometric data were divided into 25 fields covering the central regions of the LMC and eight fields in the central part of the SMC. The size of each field, both in the LMC and SMC is 35 arcmin × 35 arcmin. From the total of 33 fields, only 14 and 5 fields in the LMC and SMC, respectively, were used in the final analysis. The reason for this selection is described later in this section and discussed in the final part of the paper. The coordinates of the analyzed fields and the names are given in Table 1. The names of the fields are consistent with the OGLE-III catalog naming convention.

For each field, the color–magnitude diagram was created, and RGB stars were selected based on the $(V - K)$ color, and corresponding K band brightness. Figure 1 presents an example of the RGB stars selected on the color–magnitude diagram for field LMC127.

2.1. Edge Detection Techniques

In order to secure a precise and accurate measurement of the TRGB brightness in each field, we decided to use different techniques and investigate the results of the edge detection methods. The first method we used is the the Sobel filter, described by Lee et al. (1993), and later improved by Sakai et al. (1996). The Sobel filter is operating on the Gaussian-smoothed

Table 1
Summary Information on the 19 Analyzed Fields in the LMC and SMC

Field	R.A.	Decl.	$I_{\rm TRGB}$	$J_{\rm TRGB}$	$H_{\rm TRGB}$	$K_{\rm TRGB}$
LMC100	5:19:02.2	−69:15:07	14.581	13.254	12.343	12.103
LMC102	5:19:05.7	−68:03:46	14.661	13.382	12.459	12.252
LMC103	5:19:02.9	−69:50:26	14.615	13.255	12.353	12.104
LMC111	5:12:36.0	−69:14:50	14.714	13.328	12.342	12.114
LMC112	5:12:21.5	−69:50:21	14.602	13.273	12.382	12.093
LMC116	5:07:03.6	−67:28:25	14.682	13.350	12.493	12.247
LMC120	5:05:39.8	−69:50:28	14.643	13.302	12.426	12.179
LMC126	5:00:02.4	−68:39:31	14.620	13.313	12.442	12.153
LMC127	4:59:33.6	−69:14:54	14.638	13.325	12.416	12.204
LMC161	5:25:32.5	−69:14:59	14.624	13.267	12.373	12.154
LMC162	5:25:43.3	−69:50:24	14.579	13.234	12.323	12.085
LMC163	5:25:52.2	−70:25:50	14.648	13.298	12.392	12.134
LMC169	5:32:22.8	−69:50:26	14.691	13.284	12.392	12.095
LMC170	5:32:48.1	−70:25:53	14.600	13.242	12.358	12.123
SMC101	0:50:03.5	−72:33:03	15.017	13.894	13.062	12.871
SMC108	0:57:31.5	−72:09:29	14.972	13.901	13.055	12.894
SMC105	0:57:50.2	−72:44:35	15.081	13.955	13.113	12.945
SMC106	0:58:06.7	−73:20:21	14.995	13.904	13.051	12.875
SMC113	1:05:02.8	−72:09:32	14.994	13.851	13.042	12.817

Note. For each field, the coordinates of the center and the TRGB brightness in I, J, H, and K bands are given.

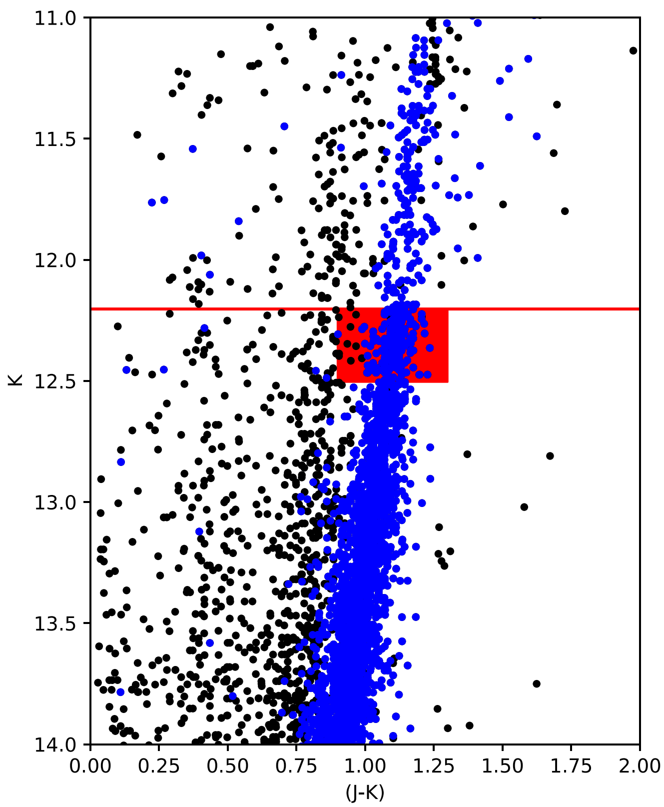

Figure 1. Example of the color–magnitude diagram for field LMC127. Blue dots represent stars of the red giant branch, which were selected based on the $(V-K)$ color and corresponding K band brightness. Red horizontal line marks the TRGB brightness measured with the PN filter, $m_{K,\ \rm TRGB} = 12.204$ mag. The red field square under the TRGB marks stars used to measure the color of the RGB.

luminosity function $\Phi(m)$, which follows the expression:

$$\Phi(m) = \sum_i^N \frac{1}{\sqrt{2\pi}\,\sigma_i} \exp\left[-\frac{(m_i - m)^2}{2\sigma_i^2}\right], \qquad (1)$$

where m_i is the magnitude of the ith star, σ_i is the ith star photometric error, and N is the total number of stars in the sample. The Sobel filter answer $E(m)$ is defined as

$$E(m) = \Phi(m + a) - \Phi(m - a), \qquad (2)$$

where a is the mean photometric error for all the stars within magnitudes $m - 0.05$ and $m + 0.05$ mag. The brightness corresponding to the highest value of the Sobel filter answer is the brightness of the TRGB. Given its simplicity, the Sobel filtering technique has been widely adopted and was employed by us in our previous papers.

While the Sobel filter is sufficient for most of the applications, in the case of some fields in the LMC and SMC, it is difficult to measure the TRGB brightness, because in the proximity of the expected cut-off on the luminosity function, the Sobel filter answer shows multiple peaks.

The second implemented method of the TRGB brightness measurement is the Maximum Likelihood Algorithm (MLA), introduced by Mendez et al. (2002) and later improved by Makarov et al. (2006). In contrast to the previously described method, in the MLA a theoretical predefined luminosity function is fitted to the observed distribution of the stars. Additionally, this method incorporates photometric errors and a completeness function. In this approach, the luminosity function is assumed to be a simple power law with a cut-off for the TRGB brightness:

$$\psi = \begin{cases} 10^{a(m-m_{\rm TRGB})+b} & \text{for } m - m_{\rm TRGB} \geqslant 0 \\ 10^{c(m-m_{\rm TRGB})} & \text{for } m - m_{\rm TRGB} < 0. \end{cases} \qquad (3)$$

Calculating the Maximum Likelihood allows us to estimate the TRGB brightness ($m_{\rm TRGB}$) and luminosity function slope parameters (a, b and c of Equation (3)). This method proved to be especially convenient if the part of the luminosity function in the proximity of the TRGB was poorly populated, or it approaches the photometric limit. Unfortunately, for many analyzed fields in the LMC and SMC, the calculated TRGB brightness differs by more than 1 mag from the expected value.

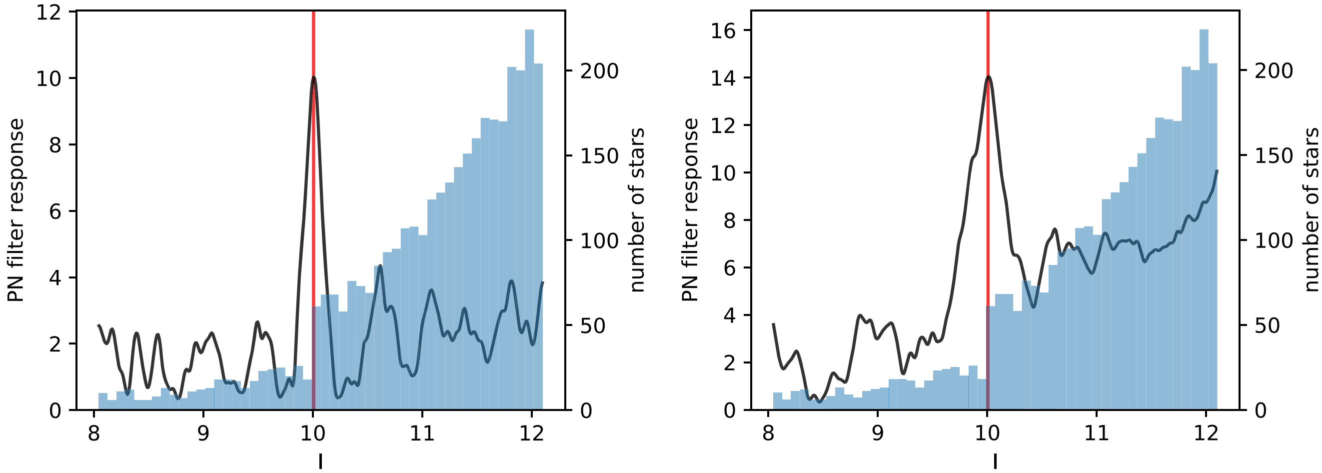

Figure 2. Example of PN detection for an artificial luminosity function. Both panels present power-law distributions with a cut-off representing the TRGB at 10 mag. Power laws were generated according to Equation (3) with slope parameters similar to those observed in the LMC ($a = 0.30$, $b = 0.30$, $c = 0.35$). In this case, the number of stars above/below the TRGB is 200/1000, which corresponds to typical values in our LMC fields. The left panel presents PN response with bin size 0.2 mag (μ parameter for Equation (4)). The right panel presents PN response with bin size 0.4 mag. It is clearly visible that for a power-law distribution with increasing bin size, the PN response value has intrinsic rising trend with increasing magnitude, which can lead to a systematic measurement error, or even prevent the detection of the TRGB.

The cause of this discrepancy is connected with an over-simplified model of the luminosity function in the case of the LMC and SMC.

Our final approach is based on the Poisson noise weighted star counts difference in two adjacent bins (hereinafter the PN method). The response of this filter is defined for any magnitude (m) with desired resolution by the following equation:

$$\mathrm{PN}(m) = \frac{(N_U - N_L)}{\sqrt{(N_U + N_L)/2}}. \tag{4}$$

N_U is the number of stars in the bin of magnitude from m to $m + \mu$, and N_L is the number of stars in the bin of magnitude from $m - \mu$ to m. The μ parameter value in our implementation was set between 0.1 and 0.3 mag, and the resolution of the calculations was set to 0.01 mag. This method was introduced with a slightly different formula by Madore et al. (2009) to statistically estimate the significance of the Sobel filer [−1, 0, +1] kernel response. In our application, we convolved the PN filter answer with a Gaussian function:

$$g(m) = \exp\left[-\frac{(m - m_0)^2}{2\sigma^2}\right]. \tag{5}$$

This procedure is used to smooth the response of the filter, which slightly improves the accuracy of the measurements, as long as the σ value does not significantly exceeds the mean photometric error of the stars. To obtain the desired smoothing, we used $\sigma = 0.03$ mag.

The main advantage of this method is the clarity of the response. Compared with the Sobel filter, the main peak is usually very distinctive, and the value of the response has a clear interpretation, since it corresponds to expected variations of the star counts number in the selected range of magnitudes. In the following subsection, we present some important properties of this filter.

2.2. PN Filter Properties

Figure 2 presents examples of the PN filter response on the artificially created power-law distribution of star magnitudes. The power law is described by Equation (3), with the edge corresponding to the TRGB at 10 mag. Parameters of the distribution are $a = 0.30$, $b = 0.30$, and $c = 0.35$, and correspond to the typical values in the LMC. Those values were calculated with the MLA technique. It is clear that for the power-law distribution, with increasing bin size μ, the PN response value has intrinsic rising trend with increasing magnitude, which can lead to a systematic measurement error. This was the main reason for us to limit the value of the μ parameter to 0.3 mag. To investigate any possible systematic errors connected with the properties of the PN filter, we performed a series of simulations. The artificial luminosity function described by Equation (3) was created with parameters $m_{\mathrm{TRGB}} = 10$ mag, and $a = 0.30$, $b = 0.30$, and $c = 0.35$. Since the main factor affecting the statistical error of the measurement is the number of stars within 1 mag above and below the TRGB, we adopted a ratio of star counts above/below the TRGB to a value typical for the LMC, that is 200/1000. We performed 10000 measurements on random generated luminosity functions, with different setups of the PN filter. We found that for a bin size value (μ in Equation (4)) from 0.2 to 0.4 mag and a σ value from 0.01 to 0.04, there is no significant difference for the distributions of the results. Figure 3 presents the results of the simulations for parameter $\mu = 0.2$ and $\mu = 0.4$ mag. Those simulations convinced us that the PN filter can be properly used to measure the TRGB brightness in the LMC and SMC.

2.3. TRGB Measurement in the LMC and SMC

Utilizing the method described in the previous subsection, we performed measurements in 19 fields in the LMC and SMC in the I, J, H, and K bands. An example of the measurement for field LMC 127 is presented in Figure 4. From the initially larger number of fields, we decided to use only measurements that were accurate and precise. The simplicity of the PN filter response makes it easy to reject measurements that provide some doubts. We decided to reject measurements if, in the proximity of the anticipated edge, there is no visually significant peak in the response of the PN filter, or if the peak

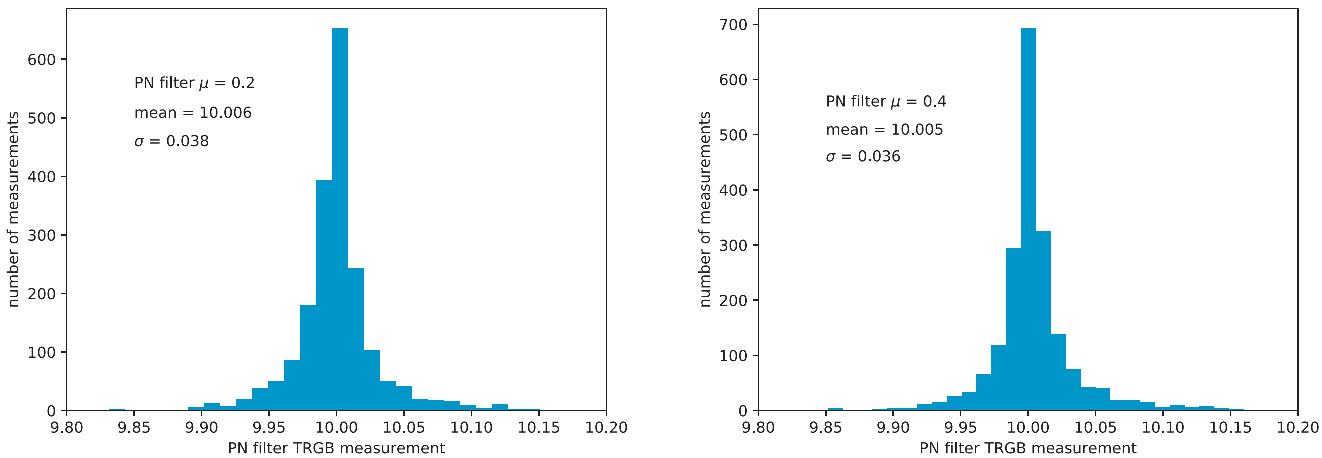

Figure 3. Distribution of the TRGB magnitude measurements of the PN filter with parameter $\mu = 0.2$ mag (left panel) and $\mu = 0.4$ mag (right panel). Each distribution was created by applying the PN filter to measure the TRGB magnitude for 2000 randomly generated artificial luminosity functions according to Equation (3). Slope parameters were set to $a = 0.30$, $b = 0.30$, and $c = 0.35$, and the number of stars above/below the TRGB was set to 200/1000. These values are typical for our analyzed fields in the LMC and were found with the MLA technique. The TRGB magnitude (m_{TRGB}) was set to 10 mag. The presented distributions prove that there is no systematic error related to application of the PN filter within used μ parameter. Both distributions have a similar standard deviation and no shift of the mean value of the distribution is observed.

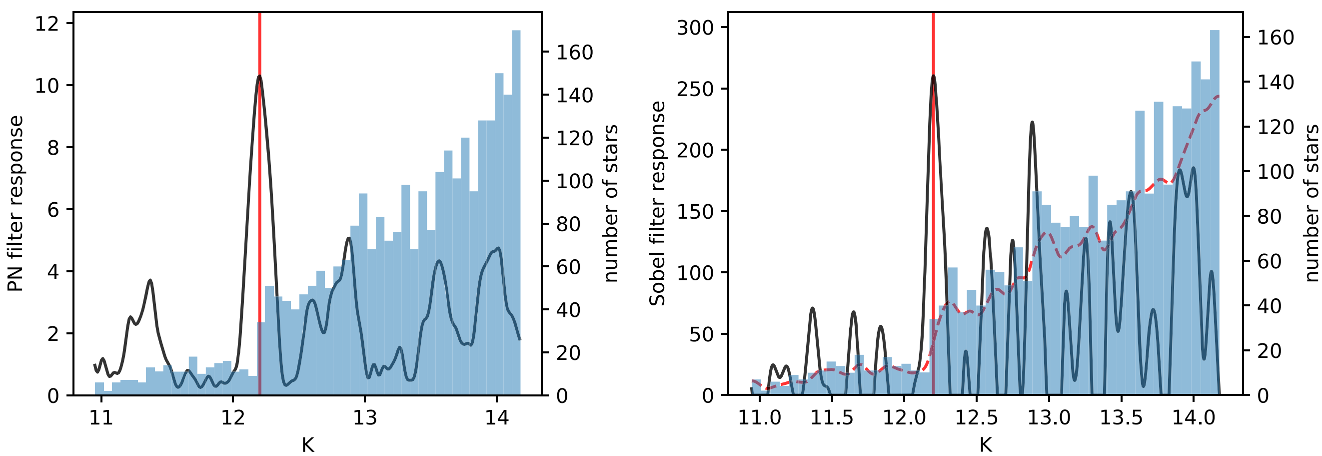

Figure 4. Example of the PN filter (left panel) and Sobel filter (right panel) application for the field LMC127. Both filters provide results that are consistent within 0.01 mag. Red vertical line marks the measured magnitude of the TRGB.

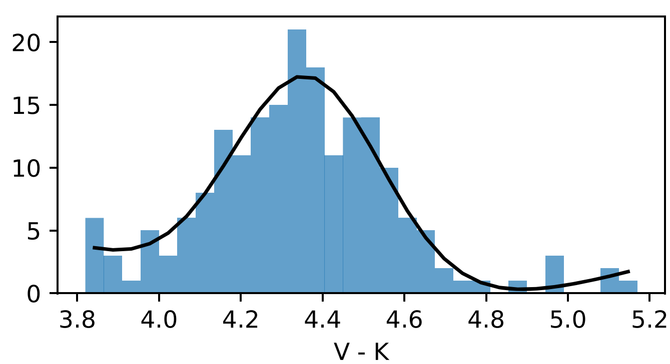

Figure 5. Example of the fit to the color of the stars in the field LMC127 according to Equation (5). Stars were selected from the red giant branch within the magnitude m, $m_{J,\mathrm{TRGB}} - m_{K,\mathrm{TRGB}} + 0.3$ mag.

has additional features, like a double maximum. We also rejected measurements if the magnitude of the maximum value changes significantly with changed μ parameter of the PN filter. It is worth noting that in all cases of measurement rejection, the Sobel filter response did not provide the possibility to measure the TRGB brightness. The statistical uncertainty of detection was estimated with a Bootstrap resampling method and was smaller than 0.04 mag in all fields.

Table 1 presents the measured values of the TRGB in the *I*, *V*, *J*, and *K* bands for the selected fields. The TRGB measurements with the Sobel filter are not given in this paper; however, they have been reported for the most of the fields earlier by Górski et al. (2016).

2.4. Color Measurement

To measure the color of the previously selected stars on the RGB, we selected stars of magnitude between measured brightness of the TRGB in the *K* band and 0.3 mag below the TRGB (stars of magnitude m, where $m_{K,\mathrm{TRGB}} < m < m_{K,\mathrm{TRGB}} + 0.3$ mag). Next we applied the fitting function (Equation (5)) to the data, which consist of a Gaussian component representing RGB stars and a second-order

Table 2
TRGB Absolute Magnitude, Unreddened Color of the Tip, Geometric Correction and Reddening in 19 Fields in the LMC and SMC

Filed	I_{TRGB}	J_{TRGB}	H_{TRGB}	K_{TRGB}	$(V-K)_0$	$(V-H)_0$	$(J-K)_0$	Geometric Correction	$E(B-V)$
LMC100	−4.087	−5.318	−6.192	−6.411	4.107	3.893	1.058	−0.004	0.110
LMC102	−4.101	−5.250	−6.122	−6.300	3.870	3.668	1.033	−0.028	0.149
LMC103	−4.047	−5.310	−6.174	−6.402	4.095	3.887	1.063	0.004	0.111
LMC111	−3.972	−5.250	−6.194	−6.399	4.085	3.868	1.060	0.002	0.124
LMC112	−4.073	−5.296	−6.146	−6.412	4.093	3.882	1.059	0.009	0.122
LMC116	−4.000	−5.240	−6.062	−6.288	3.878	3.686	1.024	−0.026	0.106
LMC120	−4.040	−5.268	−6.101	−6.323	3.997	3.792	1.047	0.015	0.130
LMC126	−4.069	−5.266	−6.094	−6.358	3.896	3.695	1.035	0.005	0.127
LMC127	−4.057	−5.250	−6.113	−6.299	3.953	3.759	1.035	0.017	0.137
LMC161	−4.091	−5.332	−6.181	−6.374	3.977	3.781	1.043	−0.010	0.134
LMC162	−4.078	−5.331	−6.207	−6.425	4.122	3.899	1.071	−0.002	0.105
LMC163	−4.041	−5.290	−6.157	−6.393	4.025	3.814	1.060	−0.014	0.116
LMC169	−4.008	−5.305	−6.155	−6.428	4.070	3.858	1.074	−0.007	0.126
LMC170	−4.093	−5.351	−6.196	−6.409	4.047	3.822	1.057	−0.020	0.115
SMC101	−4.085	−5.148	−5.956	−6.134	3.539	3.370	0.972	⋯	0.069
SMC108	−4.119	−5.135	−5.960	−6.109	3.507	3.349	0.958	⋯	0.063
SMC105	−4.035	−5.094	−5.910	−6.063	3.518	3.354	0.975	⋯	0.077
SMC106	−4.087	−5.128	−5.961	−6.126	3.558	3.396	0.974	⋯	0.058
SMC113	−4.095	−5.184	−5.972	−6.186	3.583	3.420	0.971	⋯	0.062

Table 3
Equation (5) Calibration Formula Coefficients

Band	$(V-K)_0$ −3.8	$(V-H)_0$ −3.6	$(J-K)_0$ −1.0
M_I	$a = 0.094 \pm 0.034$ $b = -4.107 \pm 0.008$	$a = 0.104 \pm 0.037$ $b = -4.109 \pm 0.008$	$a = 0.579 \pm 0.194$ $b = -4.116 \pm 0.009$
M_J	$a = -0.275 \pm 0.023$ $b = -5.264 \pm 0.006$	$a = -0.302 \pm 0.027$ $b = -5.261 \pm 0.006$	$a = -1.586 \pm 0.152$ $b = -5.241 \pm 0.007$
M_H	$a = -0.374 \pm 0.024$ $b = -6.103 \pm 0.006$	$a = -0.411 \pm 0.027$ $b = -6.097 \pm 0.006$	$a = -2.154 \pm 0.162$ $b = -6.072 \pm 0.008$
M_K	$a = -0.479 \pm 0.026$ $b = -6.304 \pm 0.006$	$a = -0.527 \pm 0.030$ $b = -6.298 \pm 0.007$	$a = -2.779 \pm 0.166$ $b = -6.264 \pm 0.008$

polynomial approximating the stellar background.

$$n(k) = a + b(k - k_0) + c(k - k_0)^2 + \frac{N}{\sigma\sqrt{2\pi}} \exp\left[-\frac{(k - k_0)^2}{2\sigma^2}\right] \tag{6}$$

where k is the color of the stars. In this paper, we used colors $(V-K)$, $(V-H)$, and $(J-K)$. Figure 5 presents an example of the fit applied to stars in field LMC127. Measured colors are reported in Table 2.

3. Calibration of the TRGB

In order to prepare the calibration of the absolute magnitude of the TRGB in terms of the unreddened colors of the RGB, we have to adopt a distance to the LMC and SMC, and interstellar extinction to both galaxies. We employ 18.493 ± 0.047 mag distance modulus to the LMC (Pietrzyński et al. 2013), which is based on eight eclipsing binary systems and is the most precise and accurate (2%) distance to this galaxy that has been determined so far. Fields analyzed in this paper are located relatively close to the center of the LMC, and the geometrical depth of the LMC should not introduce any systematic error to our calibration. Nevertheless it is one of the factors affecting the absolute magnitude of the TRGB in each field. To limit this effect, we applied the geometrical corrections calculated from the model of Van der Marel et al. (2002). Values of the geometrical corrections are reported in Table 2.

The adopted distance to the SMC is also based on the eclipsing binary method, but in this case, only five systems were used to calculate the distance (Graczyk et al. 2014). From these five systems, we decided to take into account all systems except SMC113.3 4007, which is reported to be lying outside of the main body of the galaxy by a number of studies and strongly affects the mean distance value (Matsunaga et al. 2011; Subramanian & Subramaniam 2012). Based on those four systems, the adopted distance to the SMC is 19.003 ± 0.048 mag.

Relative reddenings for our fields were calculated based on the observed $(V-I)$ colors of the red clump stars. The absolute zero-point of the reddening was adopted from the Na I D1 line and atmospheric analysis of eclipsing binaries that are located in our fields (Graczyk et al. 2014, 2018). This approach is similar to the method used by Haschke et al. (2011) and will be discussed in the following section of this paper. The adopted $E(B-V)$ reddening values are reported in Table 2. We use the Schlegel et al. (1998) $R_V = 3.1$ reddening law and a ratio of

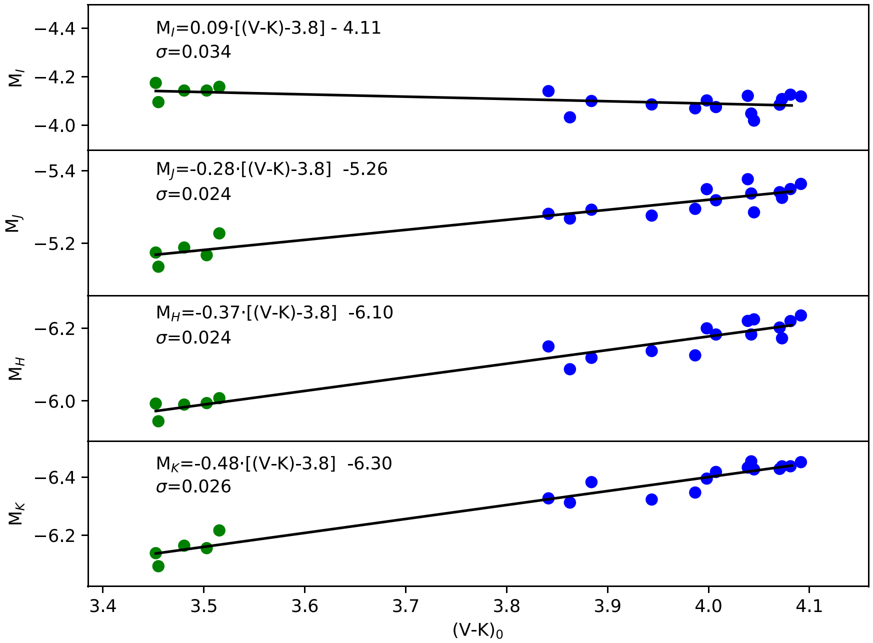

Figure 6. Absolute magnitudes of the TRGB as a function of the tip $(V-K)_0$ color. Green points come from five fields in the SMC, and blue points from 14 fields in the LMC. The black solid line is the best fit to the data.

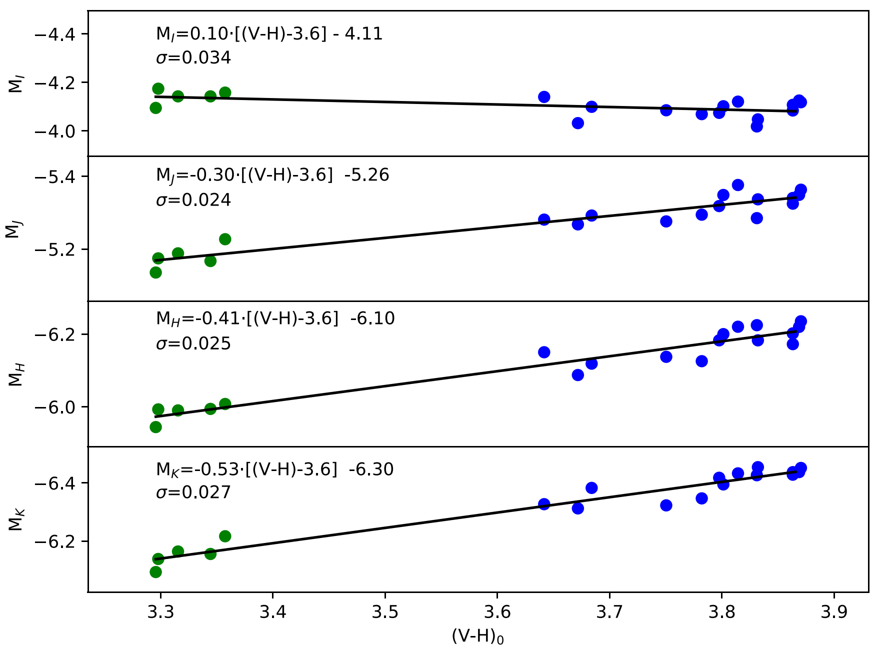

Figure 7. Absolute magnitudes of the TRGB as a function of the tip $(V-H)_0$ color. Green points come from five fields in the SMC, and blue points from 14 fields in the LMC. The black solid line is the best fit to the data.

total to selective absorption of $A_V = 1.08\ R_V$, $A_I = 0.568\ R_V$, $A_J = 0.288\ R_V$, $A_H = 0.178\ R_V$ and $A_K = 0.117\ R_V$.

To obtain the calibration of the TRGB brightness in terms of the color of the TRGB, we used the least-squares method to fit a first-order polynomial to the absolute magnitudes and unreddened colors calculated in the previous sections. The fitted relations are of the form

$$M_X = a(\mathrm{TC}_z - \mathrm{TC}_0) + b, \tag{7}$$

where M_X is the absolute magnitude of the TRGB in the band X, and TC_z is the unreddened tip color, $(V-K)_0$, $(V-H)_0$ or $(J-K)_0$. For the clarity of presented calibration formulas, we introduced TC_0 color shift ($\mathrm{TC}_0 = 3.8$ for the $(V-K)_0$, $\mathrm{TC}_0 = 3.6$ for the $(V-H)_0$ and $\mathrm{TC}_0 = 1.0$ for the $(J-K)_0$). Calculated a and b coefficients for I, J, H, and K bands for $(V-K)_0$, $(V-H)_0$ and $(J-K)_0$ tip colors are reported in Table 3. The fits are presented in Figures 6–8. Here we explicitly present calibrations of the TRGB absolute magnitude in terms of the $(V-K)_0$ color of the tip.

$$M_I = 0.09 \cdot ((V-K)_0 - 3.8) - 4.11$$
$$M_J = -0.28 \cdot ((V-K)_0 - 3.8) - 5.26$$

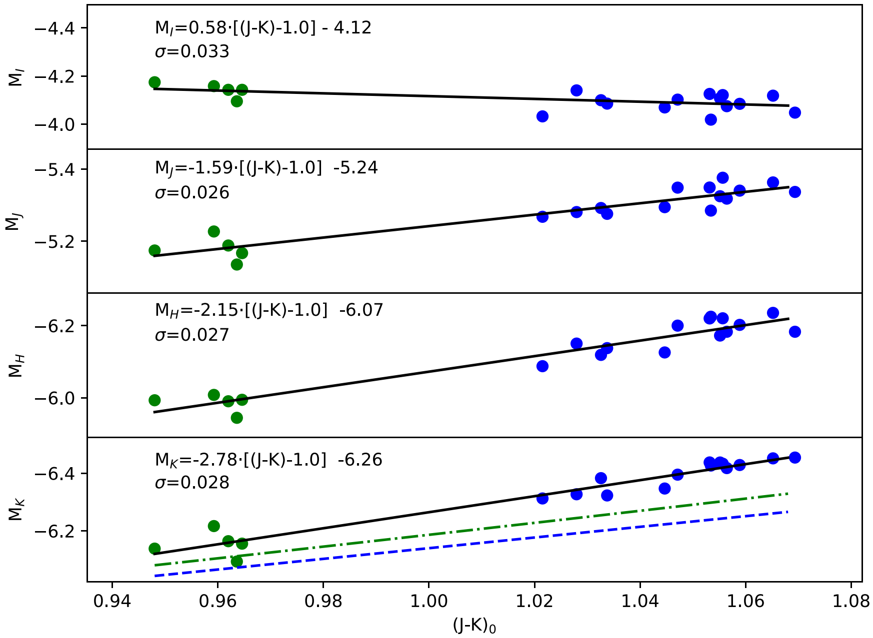

Figure 8. Absolute magnitudes of the TRGB as a function of the tip $(J-K)_0$ color. Green points come from five fields in the SMC, and blue points from 14 fields in the LMC. The black solid lines are the best fit to the data. The blue dashed line is the calibration of Hoyt et al. (2018). The green dashed–dotted line is the calibration of Serenelli et al. (2017).

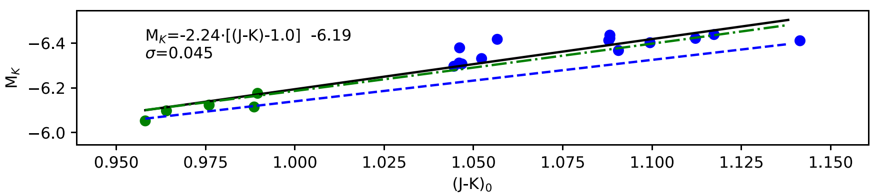

Figure 9. Absolute magnitudes of the TRGB as a function of tip color calculated as the difference of the TRGB brightness in the J and K band. Green points are five fields in the SMC, and blue points are 14 fields in the LMC. The black solid line is the best fit to the data. This approach yields different values of calibration coefficients and makes the calibration consistent with calibration of Hoyt et al. (2018)—blue dashed line, and with Serenelli et al. (2017)—green dashed–dotted line.

$$M_H = -0.37 \cdot ((V-K)_0 - 3.8) - 6.10$$
$$M_K = -0.48 \cdot ((V-K)_0 - 3.8) - 6.30.$$

4. Discussion

In this paper, we present the calibration of the optical and near-infrared brightness of the TRGB in terms of the $(V-K)$ and $(V-H)$ colors for the first time. As a complementary calibration, we provide a relation for the $(J-K)$ color, which can be compared to the results obtained by Serenelli et al. (2017) and Hoyt et al. (2018). Calibrations based on the colors of the red giants should reduce potential systematic errors observed in calibrations based on the metallicity of the stars (Salaris & Girardi 2005; Górski et al. 2016; Serenelli et al. 2017). We note that in the color range of the presented calibrations, the absolute magnitude changes least in the optical I band (0.035 mag), and in the near-infrared K band the change of the brightness of the TRGB is the strongest (0.364 mag). This basic property is in agreement with all previously published calibrations.

Our calibrations are fvalid only for the selected range of colors $3.4 < (V-K) < 4.1$, $3.2 < (V-H) < 3.9$, $0.94 < (J-K) < 1.07$. We expect that extrapolating these calibrations to a wider color range will require the use of second-order polynomials instead of the linear regression fits applied in this paper (Da Costa & Armandroff 1990; Bellazzini et al. 2001; Serenelli et al. 2017). While formally we are able to perform higher-order fits, the coefficients of the second-order term in all fits are indistinguishable from zero within a 1σ uncertainty.

To measure the TRGB brightness, we used the PN filter. For almost all analyzed fields, we were able to measure TRGB brightness with the Sobel filter as well. Using this measurement instead of the PN filter measurement does not change substantially any of our calibrations but increases the spread. As an example, using the Sobel filter measurements to calibrate the TRGB K band magnitude in terms of the $(V-K)$ color yields coefficient values of $a = -0.50 \pm 0.04$, $b = -6.28 \pm 0.01$ with a spread $\sigma = 0.041$ mag.

Color measurement performed with fitting Equation (5) secures precision and accuracy, since it distinguishes the main body of the RGB from the stellar background on the color–magnitude diagram. If we use the mean value of the color of the stars, the spread is significantly higher. We have to note that our convention of selecting stars to measure the color can introduce a significant offset because the color is effectively measured 0.15 mag below the TRGB. In fact, it is the main cause of the discrepancy between our calibration, and the calibrations of Serenelli et al. (2017) and Hoyt et al. (2018) visible in Figure 8. If instead of using measured color of the stars, we will simply take the difference of the measured TRGB brightness in the J band and measured TRGB brightness K band $(M_{J,\mathrm{TRGB}} - M_{K,\mathrm{TRGB}})$, we obtain relation virtually the same as Serenelli et al. (2017), but again with higher spread, $\sigma = 0.045$ mag (Figure 9).

The most important impact on our calibrations comes from the adopted distances to the LMC and SMC, and the adopted reddening. While the uncertainty on the LMC distance is small compared to the other contributing uncertainties, the differential distance between LMC and SMC has a significant effect on our calibration. A 0.05 mag change of the adopted SMC distance modulus yields calibration a and b coefficient changes at the level of 2σ. A corresponding effect can be attributed also to the reddening. Our reddening estimates for the analyzed fields can be compared with Haschke et al. (2011) reddening maps, and with the values obtained from the reddening law fitting to individual Cepheids in the LMC (Inno et al. 2016). Our mean reddening value agrees within 0.01 mag with values reported by Inno et al. (2016) with a standard deviation 0.04 mag. The reddening maps of Haschke et al. (2011) were obtained in a similar way that was used in this paper. In their case however, the color excess was calculated as the difference between the observed red clump color and the adopted theoretical value. If a zero-point correction of 0.065 and 0.035 is applied to the Haschke et al. (2011) reddening values to the LMC and SMC, respectively, the values of reddening in each of our fields agree within 0.01 mag.

5. Summary and Conclusions

Based on the measurements of the TRGB brightness in the optical I and near-infrared J, H, and K bands in 19 separate fields in the LMC and SMC, we derived the calibrations of the TRGB absolute magnitude in terms of the $(V-K)_0$, $(V-H)_0$, and $(J-K)_0$ color of the RGB. All calibrations are expressed in the Landolt photometric system for the optical bands, in the 2MASS photometric system for near-infrared bands. The TRGB brightness measurements were performed with a simple edge detection technique that improves the accuracy and precision of the measurements. A reddening and geometrical correction was applied to each field separately, and the best distances available to both galaxies were adopted. The $(V-K)$ color of the tip of the RGB is a robust tool allowing one to calculate the absolute magnitude of TRGB with great precision.

The research leading to these results has received funding from the European Research Council (ERC) under the European Unions Horizon 2020 research and innovation program (grant agreement No. 695099). W.G., M.G., and D.G. gratefully acknowledge financial support for this work from the Millennium Institute of Astrophysics (MAS) of the Iniciativa Cientifica Milenio del Ministerio de Economia, Fomento y Turismo de Chile, project IC120009. We (W.G., G.P., and D.G.) also very gratefully acknowledge financial support for this work from the BASAL Centro de Astrofisica y Tecnologias Afines (CATA) AFB-170002. We also acknowledge support from the IdP II 2015 0002 64 grant of the Polish Ministry of Science and Higher Education. M.G. gratefully acknowledges support from FONDECYT POSTDOCTORADO grant 3130361. Last, though certainly not least, we are grateful to the OGLE and IRSF team members for providing data of outstanding quality that made this investigation possible. We would like to thank the anonymous referee for constructive and helpful comments.

ORCID iDs

Wolfgang Gieren https://orcid.org/0000-0003-1405-9954
Dariusz Graczyk https://orcid.org/0000-0002-7355-9775
Paulina Karczmarek https://orcid.org/0000-0002-0136-0046
Bogumił Pilecki https://orcid.org/0000-0003-3861-8124
Mónica Taormina https://orcid.org/0000-0002-1560-8620

References

Baade, W. 1944a, ApJ, 100, 137
Baade, W. 1944b, ApJ, 100, 147
Barker, M. K., Sarajedini, A., & Harris, J. 2004, ApJ, 606, 869
Beaton, R. L., Freedman, W. L., Madore, B. F., et al. 2016, ApJ, 832, 210
Bellazzini, M., Ferraro, F. R., & Pancino, E. 2001, ApJ, 556, 635
Berger, T. A., Kudritzki, R.-P., & Urbaneja, M. A. 2018, ApJ, 680, 130
Cohen, R. E., Moni Bidin, C., Mauro, F., Bonatto, C., & Geisler, D. 2017, MNRAS, 464, 1874
Da Costa, G. S., & Armandroff, T. E. 1990, AJ, 100, 162
Gieren, W., Górski, M., Pietrzyński, G., et al. 2013, ApJ, 773, 69
Gieren, W., Pietrzyński, G., Nalewajko, K., et al. 2006, ApJ, 647, 1056
Gieren, W., Pietrzyński, G., Soszyński, I., et al. 2005, ApJ, 628, 695
Gieren, W., Pietrzyński, G., Soszyński, I., et al. 2009, ApJ, 700, 1141
Gieren, W., Pietrzyński, G., Szewczyk, O., et al. 2008, ApJ, 683, 611
Górski, M., Pietrzyński, G., Gieren, et al. 2016, AJ, 151, 167
Górski, M., Pietrzyński, G., & Gieren, W. 2011, AJ, 141, 194
Graczyk, D., Pietrzyński, G., Thompson, I. B., et al. 2014, ApJ, 780, 59
Graczyk, D., Pietrzyński, G., Thompson, I., et al. 2018, ApJ, 860, 1
Haschke, R., Grebel, E. K., & Duffau, S. 2011, AJ, 141, 158
Hatt, D., Freedman, W. L., Madore, B. F., et al. 2018, ApJ, 861, 104
Herrnstein, J. R., Moran, J. M., Greenhill, L. J., et al. 1999, Natur, 400, 539
Hoyt, T. J., Freedman, W. L., Madore, B. F., et al. 2018, ApJ, 858, 12
Inno, L., Bono, G., Matsunaga, N., et al. 2016, ApJ, 832, 176
Jacobs, B. A., Rizzi, L., Tully, R. B., et al. 2009, AJ, 138, 332
Jang, I. S., & Lee, M. G. 2017, ApJ, 835, 28
Karczmarek, P., Pietrzyński, G., Górski, M., et al. 2017, AJ, 154, 263
Kato, D., Nagashima, C., Nagayama, T., et al. 2007, PASJ, 59, 615
Kodric, M., Riffeser, A., Seitz, S., et al. 2015, ApJ, 799, 144
Lee, M. G., Freedman, W. L., & Madore, B. F. 1993, ApJ, 417, 553
Madore, B. F., & Freedman, W. L. 1995, AJ, 109, 1645
Madore, B. F., Freedman, W. L., Hatt, D., et al. 2018, ApJ, 858, 11
Madore, B. F., Mager, V., & Freedman, W. L. 2009, ApJ, 690, 389
Makarov, D., Makarova, L., Rizzi, L., et al. 2006, AJ, 132, 2729
Matsunaga, N., Feast, M. W., & Soszyński, I. 2011, MNRAS, 413, 223
Mendez, B., Davis, M., Moustakas, J., et al. 2002, AJ, 124, 213
Pietrzyński, G., & Gieren, W. 2002, AJ, 124, 2633
Pietrzyński, G., Gieren, W., Soszyński, I., et al. 2006, ApJ, 642, 216
Pietrzyński, G., Górski, M., Gieren, W., et al. 2009a, AJ, 138, 459
Pietrzyński, G., Górski, M., Gieren, W., et al. 2010, AJ, 140, 1038
Pietrzyński, G., Graczyk, D., Gieren, W., et al. 2013, Natur, 495, 76
Pietrzyński, G., Thompson, I. B., Graczyk, D., et al. 2009b, ApJ, 697, 862
Riess, A. G., Macri, L. M., Hoffmann, S. L., et al. 2016, ApJ, 826, 56
Rizzi, L., Tully, R. B., Makarov, D., et al. 2007, ApJ, 661, 815
Sakai, S., Madore, B., & Freedman, W. L. 1996, ApJ, 461, 713
Salaris, M., & Girardi, L. 2005, MNRAS, 357, 669
Sandage, A. 1971, ApJ, 166, 13
Schlegel, D. J., Finkbeiner, D. P., & Davis, M. 1998, ApJ, 500, 525
Serenelli, A., Weiss, A., Cassisi, S., Salaris, M., & Pietrinferni, A. 2017, A&A, 606, A33
Skrutskie, M. F., Cutri, R. M., Stiening, R., et al. 2006, AJ, 131, 1163
Soszyński, I., Gieren, W., Pietrzyński, G., et al. 2006, ApJ, 648, 375
Subramanian, S., & Subramaniam, A. 2012, ApJ, 744, 128
Szewczyk, O., Pietrzynski, G., Gieren, W., et al. 2009, AJ, 138, 1661
Tully, R. B., Courtois, H. M., & Sorce, J. G. 2016, AJ, 152, 50
Udalski, A., Soszyński, I., Szymański, M. K., et al. 2008a, AcA, 58, 89
Udalski, A., Soszyński, I., Szymański, M. K., et al. 2008b, AcA, 58, 329
Urbaneja, M. A., Kudritzki, R.-P., Bresolin, F., et al. 2008, ApJ, 684, 118
Valenti, E., Ferraro, F. R., & Origlia, L. 2004, MNRAS, 354, 815
Van der Marel, R. P., Alves, D. R., Hardy, E., & Suntzeff, N. B. 2002, AJ, 124, 2639
Wielgórski, P., Pietrzyński, G., Gieren, W., et al. 2017, ApJ, 842, 116
Zgirski, B., Gieren, W., Pietrzyński, G., et al. 2017, ApJ, 847, 88